Journal of Nuclear Materials 378 (2008) 197–210

Contents lists available at ScienceDirect

Journal of Nuclear Materials

journal homepage: www.elsevier.com/locate/jnucmat

Environmentally-assisted cracking behaviour in the transition region of an Alloy182/SA 508 Cl.2 dissimilar metal weld joint in simulated boiling water reactor normal water chemistry environment

H.P. Seifert [a,*], S. Ritter [a], T. Shoji [b], Q.J. Peng [b], Y. Takeda [b], Z.P. Lu [b]

[a] Paul Scherrer Institute (PSI), Nuclear Energy and Safety Research Department, Laboratory for Nuclear Materials, 5232 Villigen PSI, Switzerland
[b] Fracture and Reliability Research Institute (FRI), Tohoku University, Sendai, Japan

ARTICLE INFO

Article history:
Received 30 April 2008
Accepted 12 June 2008

ABSTRACT

The stress corrosion cracking (SCC) and corrosion fatigue behaviour perpendicular and parallel to the fusion line in the transition region between the Alloy 182 Nickel-base weld metal and the adjacent SA 508 Cl.2 low-alloy reactor pressure vessel (RPV) steel of a simulated dissimilar metal weld joint was investigated under boiling water reactor normal water chemistry conditions. A special emphasis was placed to the question whether a fast growing interdendritic SCC crack in the highly susceptible Alloy 182 weld metal can easily cross the fusion line and significantly propagate into the adjacent low-alloy RPV steel. Cessation of interdendritic SCC crack growth was observed in high-purity or sulphate-containing oxygenated water under constant or periodical partial unloading conditions for those parts of the crack front, which reached the fusion line. In chloride containing water, on the other hand, the interdendritic SCC crack in the Alloy 182 weld metal very easily crossed the fusion line and further propagated with a very high rate as a transgranular crack into the heat-affected zone and base metal of the adjacent low-alloy steel. The observed SCC cracking behaviour at the interface correlates excellently with the field experience of such dissimilar metal weld joints, where SCC cracking was usually confined to the Alloy 182 weld metal.

1. Introduction

Alloy 182 has been widely used as a weld filler metal to join the low-alloy steel (LAS) reactor pressure vessel (RPV) and pressure vessel nozzles to both wrought nickel-base alloys (Alloy 600) and austenitic stainless steel (304L, 316L, 316NG) components in light water reactors by manual shielded metal arc welding (SMAW). In recent years, incidents of stress corrosion cracking (SCC) in Alloy 182 in both boiling water (BWR) [1,2] and pressurized water reactors (PWR) [2,3] were reported in some countries. In the case of BWR, components such as different nozzle safe ends [1], bottom head penetration housings [4] and core shroud support welds [5] have suffered from SCC. The cracking was interdendritic (ID)/intergranular (IG)[1] and usually confined to the weld metal. None of the SCC cracks significantly penetrated the adjacent RPV base metal, which is consistent with the very high SCC resistance of LAS under light water reactor conditions [6,7]. Even after post-weld heat treatment (PWHT) significant residual stress is observed in such weld joints (see Appendix A.1) and, in particular in the context of repair welding, and has played a major role in many of these SCC incidents. Cold work from surface grinding or weld shrinkage etc. also potentially affected the SCC initiation susceptibility. The weld shrinkage strain/residual stress profile and the solidification structure (grain/dendrite boundary chemistry and misorientation) were important factors controlling the SCC crack path and propagation in weld joints [8–12].

The high SCC susceptibility of uncreviced bulk Alloy 182 weld material was also confirmed by laboratory investigations for both simulated BWR [8,13–15] and primary PWR coolant environment [16–20]. The SCC crack growth behaviour of Alloy 182 weld

Abbreviations: ANL, Argonne National Laboratory; BWM, bulk weld metal; BWR, boiling water reactor; CGR, crack growth rate; C(T), compact tension (specimen); DCPD, direct current potential drop (method); DLZ, dilution zone; DO, dissolved oxygen; DSA, dynamic strain ageing; EAC, environmentally-assisted cracking; ECP, electrochemical corrosion potential; FRI, Fracture and Reliability Research Institute; HAZ, heat-affected zone; HWC, hydrogen water chemistry; ID, interdendritic; IG, intergranular; ν, loading frequency; LAS, low-alloy steel; NWC, normal water chemistry; PPU, periodical partial unlaoding; PWHT, post-weld heat treatment; PWR, pressurized water reactor; PSI, Paul Scherrer Institute, Villigen, Switzerland; RPV, reactor pressure vessel; SCC, stress corrosion cracking; SEM, scanning electron microscope; SHE, standard hydrogen electrode; SICC, strain-induced corrosion cracking.

* Corresponding author. Tel.: +41 56 310 44 02; fax: +41 56 310 21 99.
E-mail address: hans-peter.seifert@psi.ch (H.P. Seifert).

[1] The SCC cracks usually grow along the high-angle solidification grain boundaries (see Appendix A). Because of the dendritic appearance of the corresponding fracture surface, this kind of cracking is called interdendritic in the following sections although intergranular would be the more appropriate term.

0022-3115/$ - see front matter © 2008 Elsevier B.V. All rights reserved.
doi:10.1016/j.jnucmat.2008.06.034

material and parametric effects (for the effect of ECP, sulphate/chloride, cold work, sensitization, stress intensity factor, etc.) are quite similar to those observed in wrought Alloy 600 or stainless steels, although, the higher high-temperature yield strength of Alloy 182 may make it more susceptible to SCC and low-temperature rapid crack propagation, and produce high weld residual stresses and stress intensity factors [8]. The different grain boundary chemistry of the weld metal may further increase its SCC susceptibility [8,9].

In contrast to the relatively high susceptibility of Alloy 182 to SCC growth, lab investigations revealed that LAS and their heat-affected zones (HAZ) have a very high resistance to SCC growth in chloride-free BWR environment at temperatures of 270–290 °C up to very high stress intensity factor levels of 50–70 MPa · $m^{0.5}$ (if excessive hardness > 350 HV5 is avoided by proper welding and PWHT parameters) [6,7]. It is stressed that for some very specific combinations of Alloy 182 dissimilar metal weld and cracking configurations, the residual stress can shift the stress intensity factors in the interface region to such high levels that accelerated sustained SCC in the adjacent LAS in high-purity BWR/normal water chemistry (NWC) environment cannot be fully excluded, in particular in high-sulphur LAS. These situations thus also reflect a certain safety concern.

Although many investigations on the SCC behaviour of Alloy 182 bulk weld metal [8–20] and LAS [6,7] have been performed, little attention has been paid to the SCC behaviour in the interface region between Alloy 182 and LAS, which has a complex microstructure with a potentially increased SCC susceptibility (see Appendix A). Most SCC investigations in Alloy 182 were related to the bulk weld metal [8–20] and to 'homogeneous' specimens from simplified weld configurations or weld overlays and hardly involved the interface region between Alloy 182 and LAS. The environmentally-assisted cracking (EAC) susceptibility of dissimilar welds has been screened by slow strain rate tests with smooth tensile specimens [21–25]. It is not surprising that EAC was observed in all regions under adequate testing conditions: Transgranular (TG) strain-induced corrosion cracking (SICC, [7]), e.g., occurred in the LAS in oxygenated high-temperature water and its severity was strongly dependent on the steel sulphur content. As expected, IG/ID SCC was observed in Alloy 182 weld metal in both BWR and PWR water chemistries. In several cases interface cracking along the fusion line (FL), often in conjunction with high hardness of the interface region, has been reported, thus indicating a distinct SCC susceptibility of this region. Therefore, it can be anticipated that the SCC in the transition region plays an important role in the overall SCC behaviour in the dissimilar weld joint.

In order to improve the understanding of the SCC behaviour in the transition region, in particular the SCC behaviour at the fusion line perpendicular and parallel to the fusion boundary, the SCC crack growth behaviour in the transition region of a simulated Alloy 182-SA 508 Cl.2 weld joint was investigated under simulated BWR/NWC and PWR conditions within the framework of a collaboration between the Fracture and Reliability Research Institute (FRI) of Tohoku University (Japan) and Paul Scherrer Institute (PSI, Switzerland). A special emphasis was placed to the question whether a fast growing interdendritic SCC crack in the highly susceptible Alloy 182 weld metal can easily cross the fusion line and significantly propagate into the adjacent low-alloy RPV steel or if crack arrest or interface cracking do occur at or along the fusion boundary. The following paper summarizes the most important BWR/NWC results of this joint project. In the Appendix A some important metallurgical and microstructural aspects of SCC in Alloy 182 weld metal and the interface region between the Alloy 182 weld metal and adjacent LAS are briefly summarized for the reader who is not familiar with this topic.

2. Materials and experimental procedure

The EAC crack growth behaviour under cyclic and static loading conditions in the interface region between the Alloy 182 bulk weld metal and the unaffected RPV base material of a simulated dissimilar metal weld joint was investigated in oxygenated high-temperature water at 288 °C. The EAC crack initiation and growth behaviour was thereby studied parallel and perpendicular to the fusion line in different important microstructure regions, including the bulk and dilution zone (DLZ) of the Alloy 182 weld metal, the fusion line region, as well as the HAZ and unaffected LAS base metal.

2.1. Test weld and specimens

The Alloy 182-LAS part of a dissimilar metal weld was simulated by filling a rectangular groove in a forged quenched and tempered SA 508 Cl.2 RPV steel plate by multipass SMAW (140–180 A and 22–26 V, interpass temperature < 177 °C) with Alloy 182 (Fig. 1). After welding, a PWHT at 620 °C for 24.5 h was performed, which resulted in a sensitized microstructure with massive chromium carbide precipitation on the high-angle solidification grain boundaries in the weld metal. The chemical composition and tensile test properties of the Alloy 182 weld metal and LAS base metal are summarized in Tables 1 and 2. Typical chemical composition and micro hardness profiles perpendicular to the fusion line are shown in Figs. 2 and 3.

The bulk Alloy 182 weld metal revealed a yield strength at 288 °C of 345 MPa and a SCC resistance index SCRI value of 21.3 (see Appendix A). The sulphur content of the weld metal varied between 0.007 and 0.014 wt%. The un-affected RPV base metal had a yield strength of 440 MPa and revealed a high sulphur content of 0.016 wt% and a medium susceptibility to dynamic strain ageing. The dilution zone (DLZ) in the Alloy 182 weld metal close to the fusion line with a different chemical composition than the bulk weld metal (BWM) had a thickness of 1.5–2.5 mm and a similar microstructure as the bulk weld metal. A peak micro Vickers hardness in the range of 280–320 HV0.5 was usually observed in the region of the fusion line. At some few locations, a very high peak hardness of up to 470 HV0.5 was observed in the dilution zone of the Alloy 182 weld metal in the absolute vicinity of the fusion line, which had a carbidic or martensite-like appearance. The thickness of the weld HAZ in the LAS varied between 2 to 4.5 mm and the peak

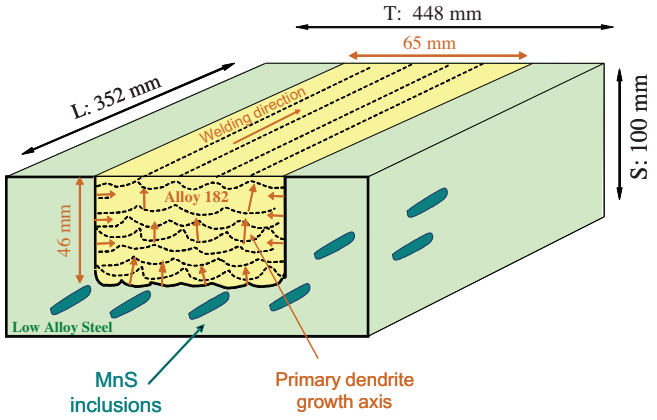

Fig. 1. Schematic of simulated Alloy 182-SA 508 Cl.2 dissimilar test weld with welding direction of individual weld beads and the orientation of the primary dendrite growth axis in the bulk weld metal and in the fusion line region. The orientation of the MnS-inclusions and the main forming direction L of the forged LAS plate are also shown.

Table 1
Chemical composition in wt% of weld filler and low-alloy RPV steel of dissimilar weld joint

Material	C	Ni	Cr	Fe	P	S	Mn	Mo	Si	Ti	Nb + Ta	Al	Co	Cu
Alloy 182 Electrode	0.04	70.8	14.26	9.7	0.002	0.003	2.46	–	0.24	0.05	1.87	–	–	0.01
Alloy 182 PSI analysis	0.043	71.6	15.1	8.3	0.002	0.07	2.85	0.45	0.2	0.027	2.19		0.04	0.01
SA 508 Cl.2 PSI analysis	0.20	0.91	0.45	96.2	0.010	0.014 0.016	0.93	0.59	0.12	–	–	0.009	0.012	0.026

Table 2
Mechanical tensile test properties of the Alloy 182 bulk weld metal and the unaffected low-alloy RPV steel

Material	T (°C)	YS (MPa)	UTS (MPa)	A_5 (%)	Z (%)
Alloy 182	288	345	547	28	50
SA 508 Cl.2	25	511	645	15.5	70.4
SA 508 Cl.2	288	440	608	12.4	70.5

YS, yield strength; UTS, ultimate tensile strength; A_5, uniform elongation; Z, reduction of area.

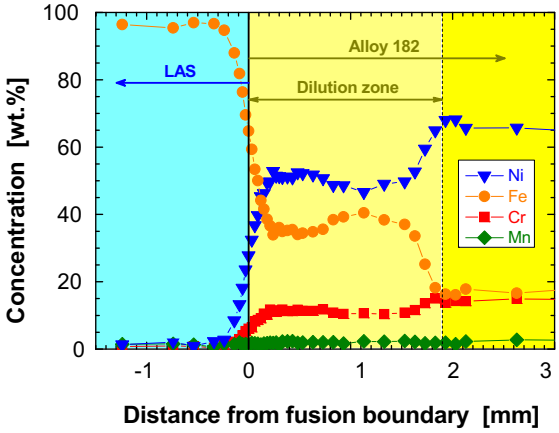

Fig. 2. Typical chemical composition profile across the fusion line.

hardness in the LAS HAZ was usually close to the fusion line and below 300 HV0.5.

Two 25 mm and fourteen 12.5 mm thick compact tension C(T) specimens with either a TS or ST orientation according to ASTM E399 [26] were cut from different locations in the test weld joint (Fig. 4 and Table 3). This involved 12 heterogeneous (Alloy 182-LAS) and 4 homogenous (bulk weld metal) specimens. The specimens either had a sharp (notch radius $\rho = 0.1$ mm) or blunt notch ($\rho = 1.5$ mm). Four specimens were additionally fatigue pre-cracked in air at room temperature with a load ratio of 0.1or 0.2 and final $K_{I,max}$ of 12–20 MPa · $m^{0.5}$.

The crack plane in the Alloy 182 weld metal was either perpendicular or parallel to the fusion line and parallel or perpendicular to the solidification direction (primary dendrite growth axis), respectively. The fatigue pre-crack-tip was either located in the bulk weld metal or in the dilution zone of the Alloy 182 at different distances from the fusion line. In the notched specimens, the notch-tip was either located at the fusion line or in the dilution zone. In all heterogeneous specimens, the MnS-inclusions were parallel to the crack front and crack plane (Figs. 1 and 4).

2.2. Experimental procedure

2.2.1. Test facilities

The EAC tests at PSI and FRI were performed in stainless steel autoclaves with integrated electromechanical loading systems, which were attached to sophisticated refreshing high-temperature

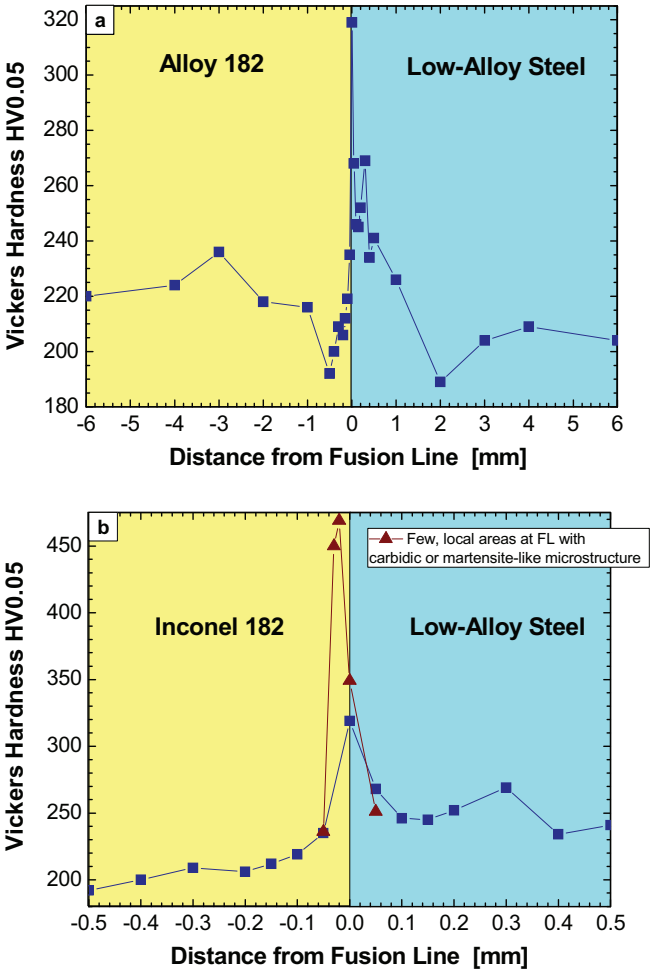

Fig. 3. Typical micro hardness profiles across the fusion line.

water loops (Fig. 5). During the experiments, all important mechanical (load, pull rod stroke) and environmental parameters at inlet and outlet (dissolved oxygen (dO), conductivity, temperature, pressure and flow) were recorded continuously. The C(T) specimens were electrically isolated from the autoclave using zirconia or oxidized zirconium alloy sleeves/spacers. The electrochemical corrosion potential (ECP) of the specimens and the redox potential (platinum probe) were continuously monitored with $Cu/Cu_2O/ZrO_2$-membrane or external Ag/AgCl/0.01 m KCl-reference electrodes. Ionic impurities of the water (inlet and outlet) were analyzed by Inductive Coupled Plasma – Atomic Emission Spectroscopy (ICP – AES) and Ion Chromatography (IC) once or twice during each test.

2.2.2. Crack length monitoring and post-test evaluations

In all but one test, crack advance was continuously monitored using the reversed direct current potential drop method (DCPD) with a resolution limit of about 1 μm in homogenous specimens. In one experiment at FRI, the alternate current potential drop

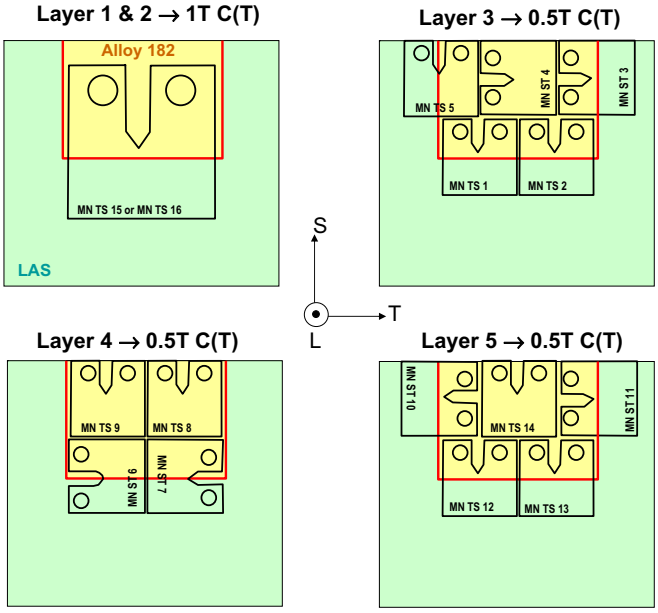

Fig. 4. Schematic of location and orientation of test specimens in the test weld.

technique (ACPD) was used. In case of the DCPD method, calibration curves were developed by a detailed 2-dimensional finite element modeling of the DC potential field for the specific bimetallic weld joint specimen/DCPD system configuration [27], since the Johnson formula would significantly underestimate the real crack growth increment in the dissimilar metal welds. The DCPD crack growth results were linearly corrected with the average EAC crack increment measured on the fracture surface at 50 equidistant locations. In spite of the finite element calibration of the DCPD, the heterogeneous specimens involved correction factors of 10 to 50%, which were related to the wavy shape of the fusion line, uneven crack fronts, out-of-mid-plane cracking at the fusion line and in particular to the very high roughness of the fracture surfaces.

After the test, the specimens were broken apart by fatigue for post-test evaluation. The fracture surface, cracking mode and position of the crack-tip were analyzed by optical and scanning electron microscope (SEM) as well as with energy-dispersive X-ray microanalysis (EDX). The fatigue pre-crack/final crack length and EAC growth increments were measured on the fracture surface at 50 equidistant locations by optical microscope or SEM. For detailed fractographical analysis of the LAS part, the oxide film on the fracture surface of one specimen half was removed by galvanostatic reduction in an ENDOX-bath [28].

Cross sections perpendicular to the crack plane were cut from the specimens for micro-hardness measurements and detailed metallographical characterization (microstructure, inclusions, crack-path, branching and secondary cracking, etc.) by optical microscope and SEM/EDX. The cross-sections were polished and chemically and electrochemically etched by several different procedures to reveal the different microstructural features in the different regions of the weld joint.

Further metallographic specimens were directly cut from the weld joint for additional analyses of the microstructure, element-composition and micro-hardness across the fusion line.

2.2.3. Environmental conditions

The EAC tests were performed in oxygenated high-purity high-temperature water at 288 °C under low-flow conditions (4 to 8 autoclave exchanges per hour, local flow rate of some few mm/s). In several cases chloride (50 ppb Cl^- as NaCl) or sulphate (30 ppb SO_4^{2-} as H_2SO_4 or Na_2SO_4) was added to reduce the crack initiation time or to accelerate crack growth. A DO content of 0.2 and 0.4 ppm or an increased level of 2 and 8 ppm were used, respectively. The lower DO levels represent a realistic simulation of the total oxidant concentration in the reactor water, whereas the increased DO contents were used to simulate a realistic ECP at Alloy 182 attachment welds within the RPV. The ECP of the heterogeneous specimens of +50–+70 (0.2 or 0.4 ppm DO) and +130–+170 mV_{SHE} (2 or 8 ppm DO) were between the typical values observed in homogeneous LAS and nickel-base alloys at PSI. The corresponding redox potentials of the environment were +250–+270 mV_{SHE} (0.2 or 0.4 ppm DO) and +290–+300 mV_{SHE} (2 or 8 ppm DO).

2.2.4. Loading conditions

Before applying the different loading sequences, the specimens were usually pre-oxidized in the test environment at a small constant pre-load of 0.5 kN ($K_I \leqslant 2$ MPa · $m^{0.5}$ in case of pre-cracked specimens) for at least one week in order to achieve stable environmental and electrochemical conditions.

In case of pre-cracked specimens with the pre-crack-tip in the bulk or dilution zone of the Alloy 182 weld metal, the following complex initial loading procedure was first applied to achieve a complete transdendritic → interdendritic transitioning along the whole crack front and to evolve a plastic zone, which is characteristic for a growing SCC crack:

Table 3
Overview on investigated heterogeneous dissimilar metal weld specimens

Specimen designation	Type of specimen	Type of notch	Location of notch ground or pre-crack-tip	Orientation of crack plane and growth direction with respect to FL & SD
MN TS 1	0.5T C(T)	Air fatigue pre-crack	DLZ at 0.5 mm from FL	⊥ to FL and ∥ to SD
MN TS 2	0.5T C(T)	Air fatigue pre-crack	DLZ at 0.6 mm from FL	⊥ to FL and ∥ to SD
MN ST 3	0.5T C(T)	Sharp notch, ρ = 0.1 mm	DLZ at 0.8 mm from FL	⊥ to FL and ∥ to SD
MN TS 5	0.5T C(T)	Sharp notch, ρ = 0.1 mm	LAS HAZ	∥ to FL
MN ST 6	0.5T BNC(T)	Blunt notch, ρ = 1.5 mm	FL with specimen mid-plane at fusion interface	∥ to FL and ⊥ to SD
MN ST 7	0.5T C(T)	Sharp notch, ρ = 0.1 mm	FL with specimen mid-plane at fusion interface	∥ to FL and ⊥ to SD
MN ST 10	0.5T C(T)	Sharp notch, ρ = 0.1 mm	DLZ at 0.9 mm from FL	⊥ to FL and ∥ to SD
MN ST 11	0.5T C(T)	Sharp notch, ρ = 0.1 mm	DLZ at 0.9 mm from FL	⊥ to FL and ∥ to SD
MN TS 12	0.5T C(T)	Sharp notch, ρ = 0.1 mm	DLZ at 0.9 mm from FL	⊥ to FL and ∥ to SD
MN TS 13	0.5T C(T)	Sharp notch, ρ = 0.1 mm	DLZ at 1.5 mm from FL	⊥ to FL and ∥ to SD
MN TS 15	1 T C(T)	Air fatigue pre-crack	DLZ at 1.5 mm from FL	⊥ to FL and ∥ to SD
MN TS 16	1 T C(T)	Air fatigue pre-crack	BWM at 3 mm of FL	⊥ to FL and ∥ to SD

DLZ, dilution zone of Alloy 182 weld metal; BWM, Alloy 182 bulk weld metal; LAS HAZ, heat-affected zone of low-alloy steel; FL, fusion line; SD, solidification direction – primary dendrite growth axis.

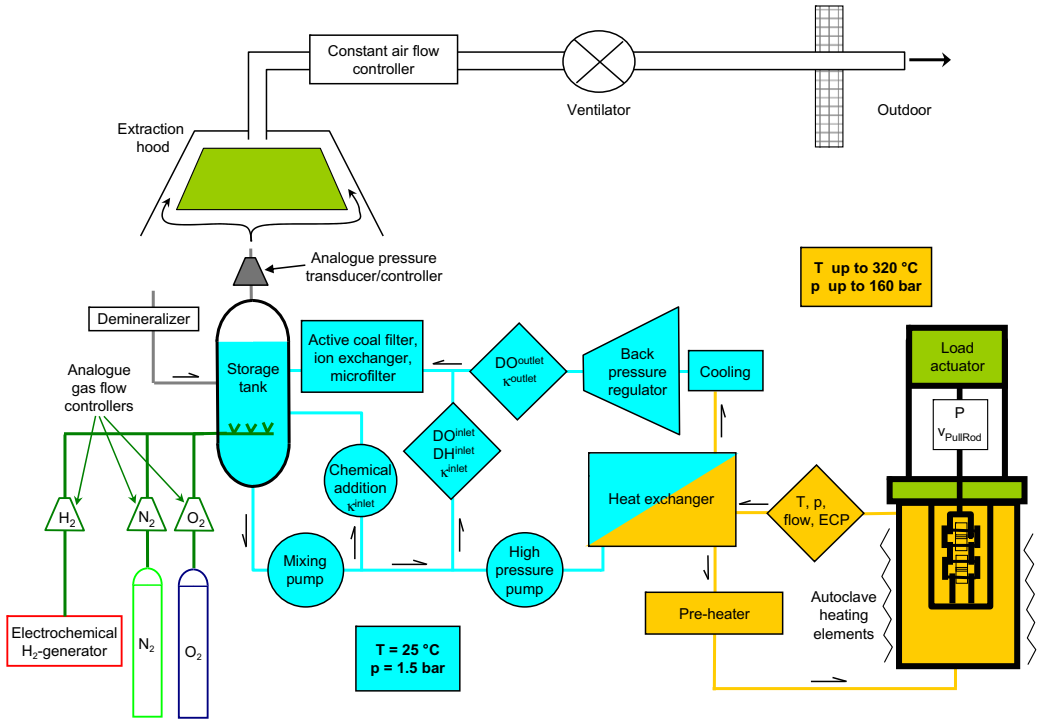

Fig. 5. Schematic of the refreshing water loop with autoclave and integrated electro-mechanical tensile machine.

1. Cyclic loading, stepwise increase of R from 0.3 to 0.7 at 0.01–0.036 Hz.
2. Cyclic loading at $R = 0.7$ with stepwise decrease of ν from 0.02 to 0.001 Hz.
3. Ceriodical partial unloading (PPU) at $R = 0.7$, $\Delta t_{hold} = 9000$ s, $\Delta t_{trise} = \Delta t_{decline} = 500$ s.
4. Constant load or near constant load (PPU wit $\Delta t_{hold} = 24$ h) with a target K_I or $K_{I,max}$ value of 25 to 35 MPa · $m^{0.5}$.

There were some slight variations in loading step 1 and 2 in some experiments, but this did not affect the crack growth results in the subsequent loading phases. After this initial loading procedure, constant or periodical partial unloading loading was kept during the whole remaining test period until unloading in some experiments. In some other tests, this phase was followed by several sequences of cyclic, periodical partial unloading and static loading to study the crack growth behavior in different microstructure regions of the weld joint. In order to reduce the total testing time, the applied stress intensity factor was sometimes increased stepwise.

In case of experiments, which started with a sharp or blunt notch, the cyclic loading started with a low load ratio of 0.065 and a frequency of 0.036 Hz. The subsequent loading phases were identical to those described above.

The $K_{I,max}$ values were varied between 20 and 60 MPa · $m^{0.5}$. With few exceptions, these values were below the ASTM E647 limit [29] in case of cyclic loading and the ASTM E1681 limits [30] in case of periodical partial unloading or constant loading conditions.

The SCC crack growth results were then compared with a Swedish disposition line for Alloy 182 [31] and the EPRI BWRVIP-60 SCC line for LAS [32]. The corrosion fatigue crack initiation results were compared to the ASME III mean curve for austenitic alloys and LAS [33–35]. For this reason a pseudo elastic notch stress range $\Delta\sigma = 2 \cdot S_a = \Delta K/\sqrt{\rho}$ was calculated for comparison purposes [36]. The corrosion fatigue crack growth behaviour was analyzed in the time domain and compared to a PSI BWR/NWC curve for LAS [7,37] and a curve developed by Argonne National Laboratory (ANL) for wrought Alloy 600 [39]. The corresponding air fatigue crack growth rates in the LAS and Alloy 182 were estimated based on [38] and [39], respectively.

3. Results and discussion

In the following paragraphs, the main observations of these complex investigations are summarized and illustrated by some selected test results. In the first two sub-sections, the SCC and EAC crack growth behaviour perpendicular and parallel to the fusion line is discussed. This is followed by a short summary of the SCC crack growth in Alloy 182 bulk weld metal. Finally, the corrosion fatigue initiation and growth behaviour in the Alloy 182 weld metal and at the fusion line is briefly outlined.

3.1. SCC crack growth behaviour perpendicular to the fusion line

The SCC behaviour perpendicular to the fusion line was investigated under periodical partial unloading or constant load with fatigue pre-cracked 25 and 12.5 mm thick C(T) specimens at PSI and FRI in high-purity water and water with 30 ppb of sulphate or 50 ppb of chloride. The fatigue pre-crack-tips in the different specimens were located either in the bulk or the dilution zone of the Alloy 182 weld metal at a mean distance between 3 and 0.5 mm from the fusion line.

As expected, fast interdendritic SCC was observed in the Alloy 182 bulk weld metal parallel to the solidification direction in oxygenated, high-purity high-temperature water in the typical range of other investigations [8,14,40] (Fig. 6) and slightly below the Swedish SCC disposition line for Alloy 182. The subsequent SCC crack growth rates in the Alloy 182 dilution zone were similar to those of the bulk weld metal and tended to slightly decrease with decreasing distance to the fusion line (Fig. 7). The corresponding SCC crack growth rates in oxygenated high-temperature water with 50 ppb Cl^- or 30 ppb SO_4^{2-} were about a factor of 10 and 5

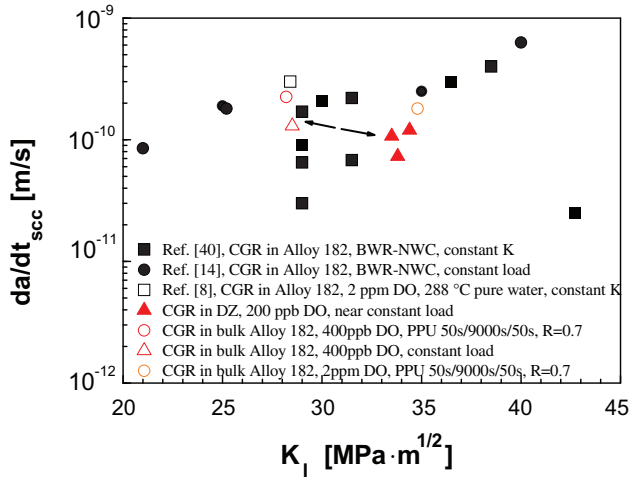

Fig. 6. Similar SCC crack growth rates in the bulk and dilution zone of the Alloy 182 weld metal in the heterogeneous dissimilar metal weld specimens as in other comparable investigations with homogeneous Alloy 182 specimens under BWR/NWC conditions [8,14,40].

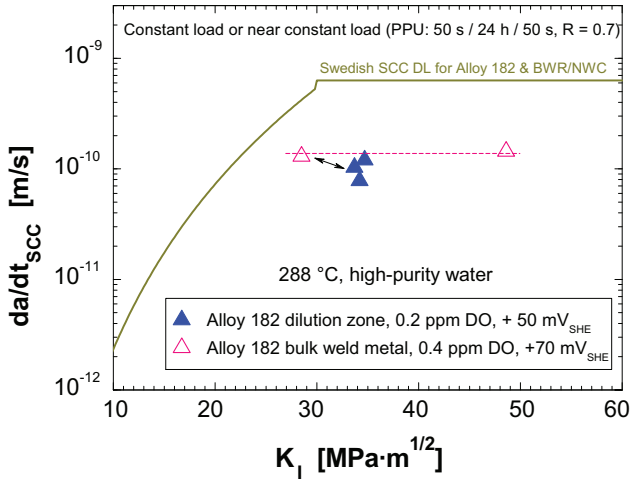

Fig. 7. Similar SCC crack growth rates in the Alloy 182 dilution zone and bulk weld metal of the weld joint.

higher than in high-purity water and slightly higher than the Swedish SCC disposition line for Alloy 182 (Fig. 26 in Section 3.3).

Cessation of SCC was observed in high-purity or sulphate-containing water in all tests under periodical partial unloading or constant load conditions for those parts of the crack front, which reached the fusion line. As soon as the overwhelming part of the crack front has reached the fusion line, a drastic drop of interdendritic SCC crack growth rates (Figs. 8 and 9) was observed even under aggressive environmental conditions (8 ppm DO and 30 ppb SO_4^{2-}) and crack arrest occurred at or close to the fusion line (Figs. 9(b), 10, 11). Crack arrest at the fusion line was confirmed in one test with periodical partial unloading, which was running for further 800 hours after the DCPD had indicated cessation of crack growth close to the fusion line (i.e., $da/dt_{SCC} < 1 \times 10^{-11}$ m/s). Minor crack growth (< 60 μm) into the heat-affected zone of the RPV steels with subsequent crack arrest was observed at some few, very localized regions along the crack front, in some specimens. On the other hand, at several locations along the crack front crack branching and deflection of EAC crack growth (up to some few 100 mm) along the fusion line in the dilution zone of Alloy 182 in the direct vicinity of the fusion boundary was a quite common observation in most

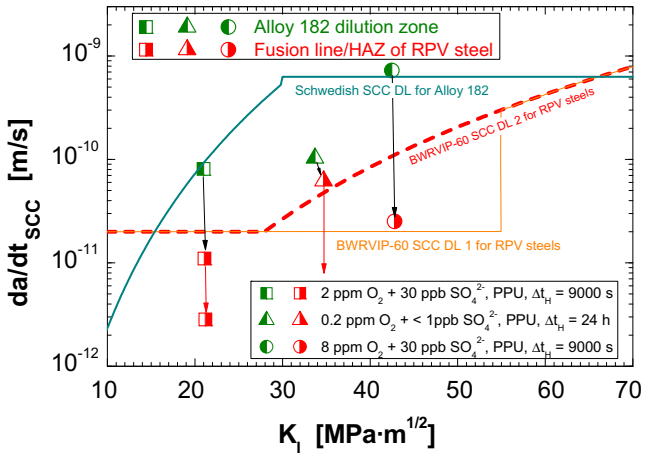

Fig. 8. Cessation of SCC crack growth at the fusion boundary under periodical partial unloading conditions in specimens MN TS 1, MN TS15 and MN TS 16. Comparison of the SCC crack growth rates in the interface region with a Swedish disposition line for Alloy 182 weld metals [31] and with the BWRVIP-60 SCC disposition lines for LAS [32].

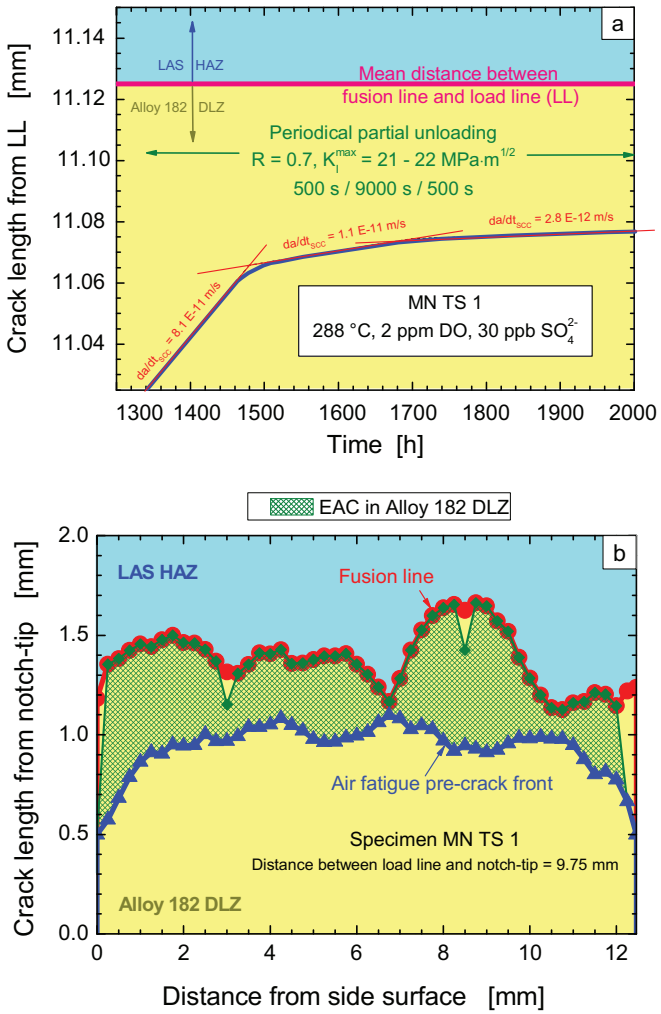

Fig. 9. (a) Cessation of SCC under periodical partial unloading in the Alloy 182-fusion line region in specimen MN TS 1 indicated by DCPD. (b) In spite of the fact that the periodical partial unloading was sustained for further 800 hours after indication of crack arrest by DCPD, the SCC crack did not enter to the adjacent LAS as independently confirmed by post-test fractography in the SEM/EDX.

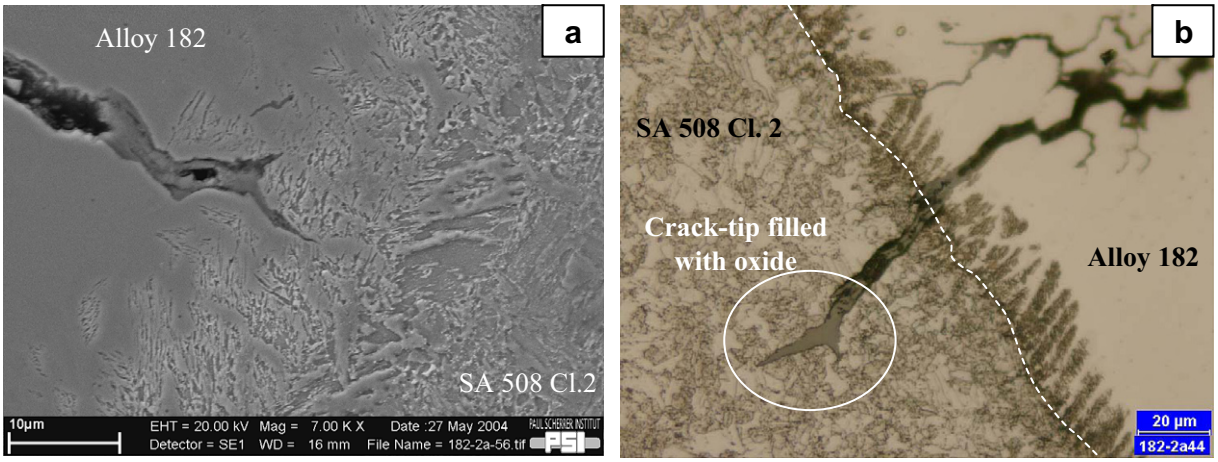

Fig. 10. Confirmation of cessation of SCC at (a) or close to the fusion boundary (b) by etched cross sections of specimens MN TS 1 and MN TS 2. The 'Nital' etching only attacks the LAS, but not the Ni-base weld metal.

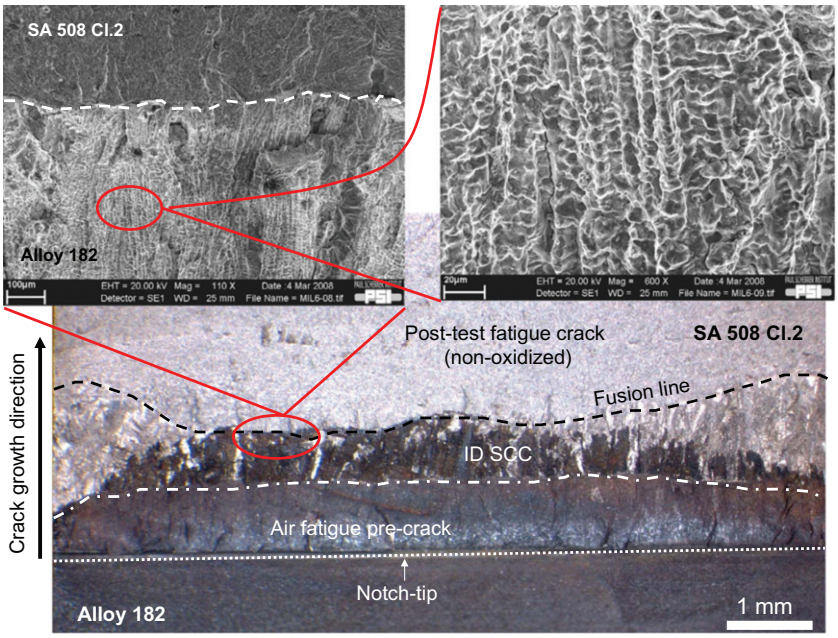

Fig. 11. Confirmation of cessation of interdendritic SCC in the fusion line region by post-test fractography of specimen MN TS 2 in the LM and SEM.

specimens, which indicates an increased SCC susceptibility of this region.

After cessation of EAC crack growth under periodical partial unloading at the fusion boundary in high-temperature water with 30 ppb of sulphate, the crack was forced to cross the fusion line by severe cyclic loading under aggressive environmental conditions in one specimen. Even in case of severe cyclic loading, the crack had problems to cross the fusion line and rather tended to grow in the Alloy 182 dilution zone along the fusion line before it finally entered into the RPV steel [Fig. 12(a)]. This again indicates an increased EAC susceptibility of the interface region parallel and close to the fusion line in the dilution zone of the weld metal. After crossing of the fusion line under severe cyclic loading conditions, the EAC crack growth rates under periodical partial unloading in the LAS HAZ were more than one order of magnitude lower than in the Alloy 182 bulk weld material. Suddenly after switching from periodical partial unloading to constant load, cessation of SCC and crack arrest occurred in both the LAS HAZ and bulk LAS in spite of the high applied stress intensity factors and aggressive environmental conditions (Fig. 13). The EAC crack growth in the un-affected LAS thus only grew under cyclic load (or during the slow rising load phase of the periodical partial unloading) by corrosion fatigue (or strain-induced corrosion cracking), but not by SCC under pure static loading. The corrosion fatigue rates were thereby in the typical range for homogenous LAS base metal and LAS HAZ specimens from other PSI investigations [7,37] (Fig. 14). The Alloy 182 bulk weld material and the bulk LAS of the bimetallic weld joint specimen therefore behaved exactly in the same manner as corresponding materials in homogeneous specimens.

In contrast to high-purity or sulphate containing oxygenated water, the interdendritic SCC in the Alloy 182 weld metal in high-temperature water with 50 ppb of chloride very easily crossed the fusion line straight forward on the same plane under periodical partial unloading and constant loading conditions (Figs. 12(b), 15 and 16) with very minor cracking along the interface. In the LAS HAZ and LAS base metal the crack grew with an extremely high rate under constant load. The SCC rates were thereby in the typical range of similar PSI investigations with chloride impurities and homogeneous LAS specimens (Fig. 17) [7]. The same observation was also made under cyclic load in chloride containing water

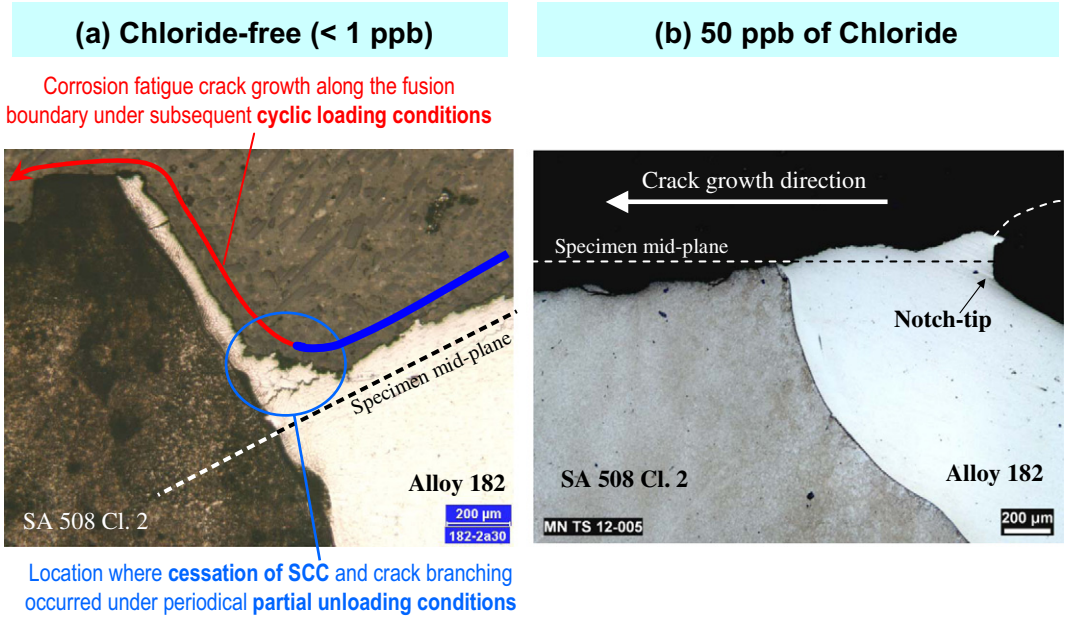

Fig. 12. Illustration of the fundamentally different EAC behaviour in the interface region perpendicular to the fusion line in high-temperature water with < 1 ppb (a) and 50 ppb chloride (b) by polished and etched cross sections.

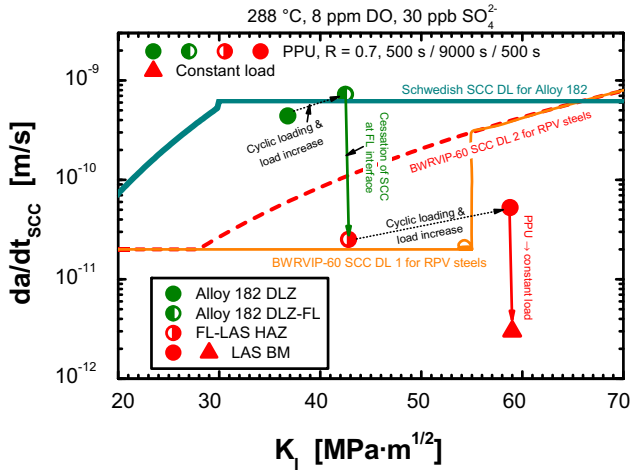

Fig. 13. Comparison of SCC crack growth rates in the fusion line – LAS HAZ region and in the unaffected LAS base metal in specimen MN TS 15 after crossing the fusion line by severe cyclic loading [see also Fig. 12(a)] with SCC disposition lines for Alloy 182 [31] and LAS [32].

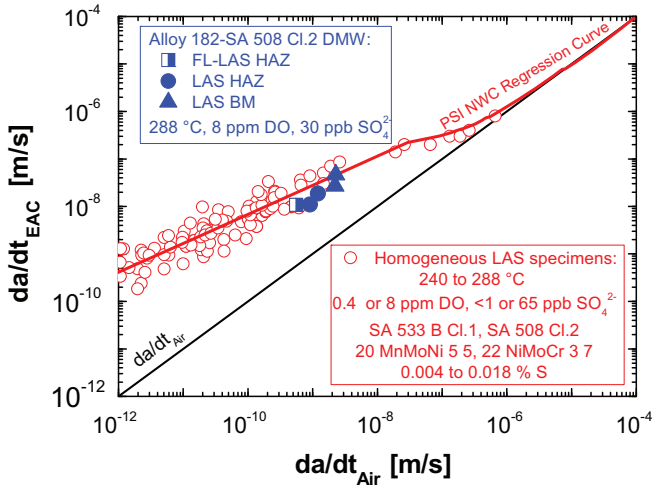

Fig. 14. Comparable corrosion fatigue crack growth rates in LAS HAZ and base metal of specimen MN TS 15 with PSI results from homogeneous LAS specimens [7,37].

[37]. The trans- or mixed inter-/transdendritic corrosion fatigue crack also very easily crossed the fusion line under cyclic load and further propagated along a transgranular path in the LAS HAZ. The corrosion fatigue crack growth rates were thereby in the typical range for LAS under similar system conditions [7,37]. It was thus clearly demonstrated, that in contrast to high-purity or sulphate containing high-temperature water, a growing mixed trans-/interdendritic corrosion fatigue and interdendritic SCC crack in the Alloy 182 weld metal can very easily cross the fusion line under both cyclic or static load in case of chloride impurities in the reactor coolant.

3.2. SCC initiation and crack growth behaviour parallel to the fusion line

The EAC behaviour parallel to the fusion line was investigated with notched 12.5 mm thick 0.5 T C(T) specimens, which either had a sharp (ρ = 0.1 mm) or a blunt (ρ = 1.5 mm) circular notch and which were pre-cracked in the test environment under cyclic load. The notch-tip was located in the Alloy 182 dilution zone in the vicinity of the fusion line. The plane of the subsequent EAC crack growth was parallel to the fusion line and perpendicular to the solidification direction (and primary dendrite axis) of the Alloy 182 weld metal.

In case of the sharp notch, the crack initiated at the notch-tip in the dilution zone of the Alloy 182 weld metal by fatigue with no (high-purity water) or only minor (50 ppb Cl^-) environmental effects (Fig. 18). After a crack advance of about 200 µm, stationary 'long crack' growth behaviour was observed. As shown schematically in Fig. 19(a), the crack grew transdendritically by corrosion fatigue parallel to the fusion line (perpendicular to the solidification direction). The environmental acceleration of corrosion fatigue increased with decreasing loading frequency (Fig. 20). The corresponding corrosion fatigue crack growth rates were in the same

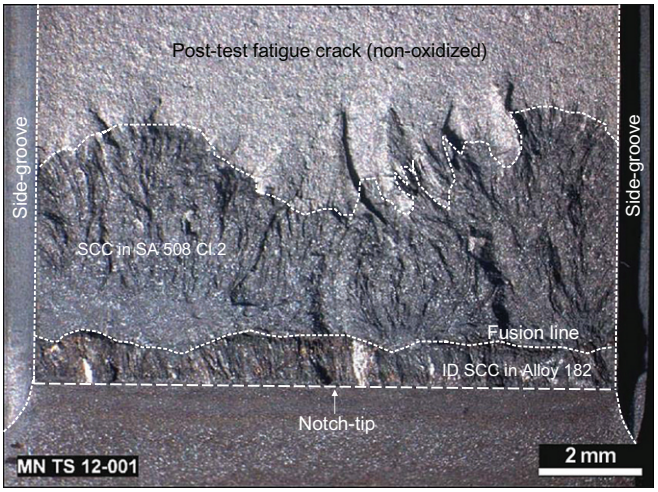

Fig. 15. Fracture surface of specimen MN TS 12 with ID SCC in Alloy 182 and TG SCC in the LAS HAZ and base metal from a test in high-temperature water with 2 ppm DO and 50 ppb of chloride.

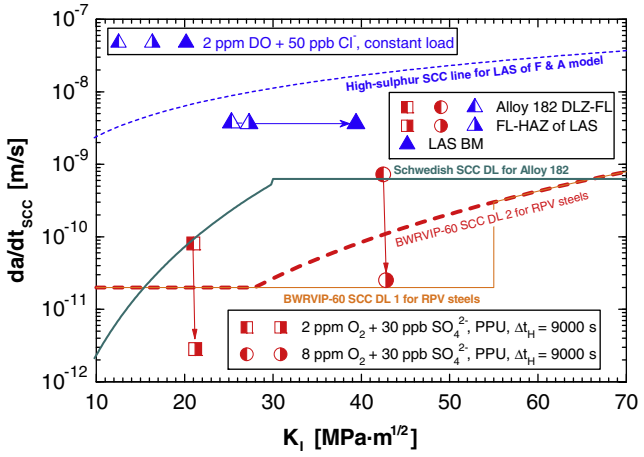

Fig. 16. Comparison of the fundamentally different SCC behaviour in the interface region in high-temperature with sulphate and chloride.

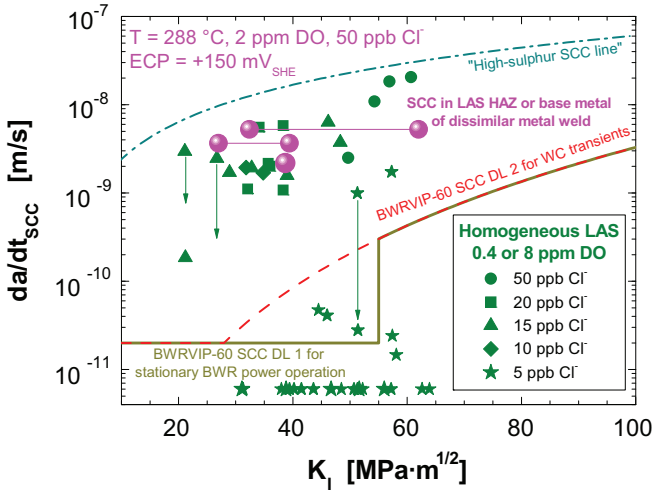

Fig. 17. Comparison of SCC growth rates in the LAS HAZ and base metal of the dissimilar test weld with PSI results from homogeneous LAS specimens in case of increased chloride contents [7].

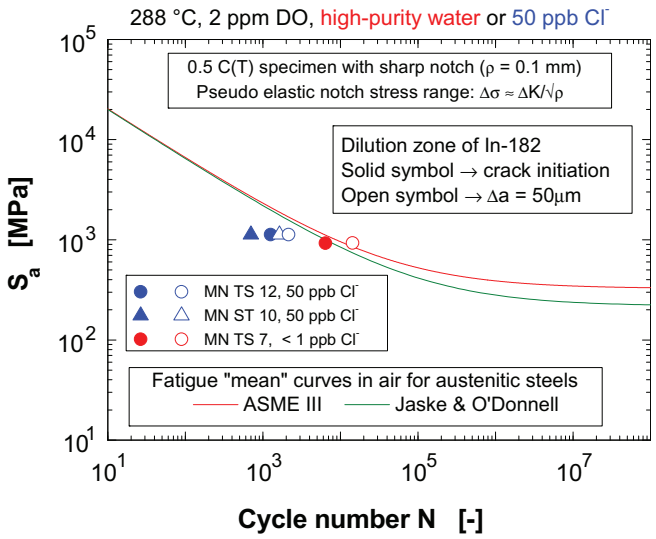

Fig. 18. Comparison of fatigue initiation in Alloy 182 dilution zone in oxygenated high-temperature water with ASME III air mean curve for austenitic steels [33–35].

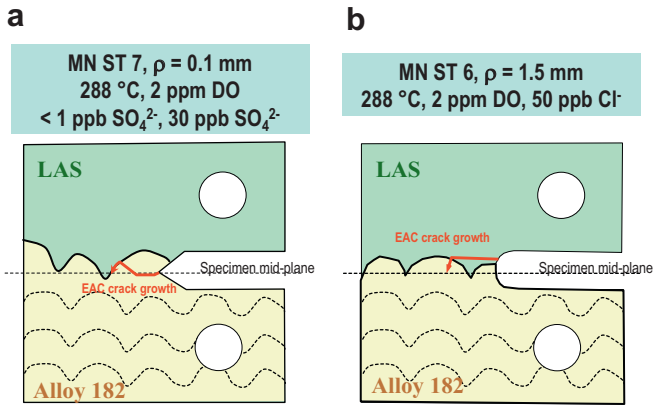

Fig. 19. Schematic of EAC path in specimens MN ST 7 (a) and MN ST 6 (b) with crack planes parallel to fusion line and notch-tips at fusion boundary.

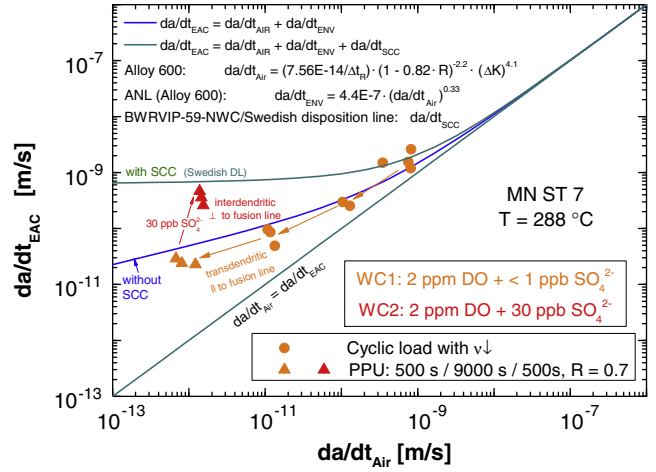

Fig. 20. Comparison of the transdendritic corrosion fatigue crack growth rates in specimen MN ST 7 in the dilution zone of Alloy 182 weld metal parallel to the fusion line under cyclic and periodical partial unloading in oxygenated high-temperature water with the ANL corrosion fatigue curve for Alloy 600 [39]. Furthermore, the subsequent interdendritic SCC rates perpendicular to the fusion line under periodical partial unloading are compared with a modified ANL-curve with an additional SCC contribution.

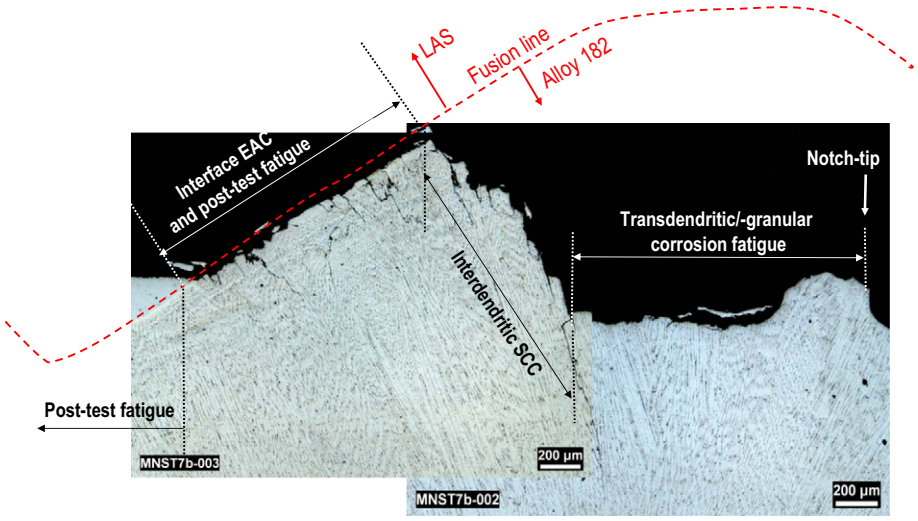

Fig. 21. Polished and etched cross section of Alloy 182 half of specimen MN ST 7 [see Figs. 19(a) and 20].

range as the ANL-curve for Alloy 600 [39] and a factor of 5–10 lower than typical interdendritic corrosion fatigue rates perpendicular to the fusion line (parallel to the solidification direction) under identical loading and environmental conditions (see Fig. 27 in Section 3.4). The transdendritic EAC crack growth rates under subsequent periodical partial unloading confirmed the absence of any significant SCC contribution during the constant load periods (Fig. 20). Briefly after addition of 30 ppb of sulphate, deflection of crack growth from its original path occurred under periodical partial unloading and the crack grew interdendritically along the solidification direction towards the fusion line by SCC (Figs. 19(a), 20 and 21). The SCC crack growth rates were thereby in the typical range for Alloy 182 for this K_I-level and environmental conditions. When the crack front reached the fusion line, crack arrest occurred at most locations at the fusion boundary, but in some isolated regions the crack further grew along the fusion boundary, which further confirmed the previous observations once more (Fig. 21).

The basic idea of the corresponding test with the blunt notch specimen (ρ = 1.5 mm) was that the crack can initiate in and easily grow along the most susceptible microstructure region. In this test, 50 ppb chloride was added from the beginning of the experiment to reduce the required crack initiation time. Although the mid-plane of the specimen was located in the dilution zone of Alloy 182 very close to the fusion line, the crack initiated in the HAZ of the LAS by corrosion fatigue [Fig. 19(b)]. This indicates a higher corrosion fatigue susceptibility of the LAS with respect to the Alloy 182 weld metal under these environmental and loading conditions, which is not surprising. It is stressed that the situation might be opposite under pure static loading conditions as shown by service experience, in particular in high-purity water without chloride. Unfortunately, typical SCC initiation times of one to several years make such investigations under lab/project conditions impossible. With respect to air environment the number of cycles to crack initiation was drastically reduced by the action of the test environment as it is expected for LAS under these conditions (Fig. 22) [34].

Subsequent to initiation, the corrosion fatigue crack growth rate in the LAS HAZ continuously accelerated. After a crack advance of about 400 µm, stationary transgranular corrosion fatigue crack growth with a rate in the range of the low-sulphur line of the Ford & Andresen EAC model [41,42] was observed (which might be related to the fact that only few MnS-inclusions were intersected by the short crack enclave). With further crack growth and decreasing loading frequency the environmental acceleration of corrosion fatigue crack growth in the LAS HAZ increased and the corrosion fatigue crack growth rates shifted towards the typical PSI long-crack corrosion fatigue data [7,37] of homogeneous LAS specimens under NWC conditions (Fig. 23). The corrosion fatigue crack grew parallel to the specimen mid-plane and therefore slowly approached the fusion line because of its wavy form (through the sequence of the individual weld beads). After switching to periodical partial unloading the crack in the LAS HAZ grew by SCC with a high rate, which was in the typical range for LAS in chloride-containing, oxygenated high-temperature water (Fig. 17). Close to the fusion line, constant load was applied and the transgranular crack further grew with a fast SCC rate. When the crack front reached the fusion line, it easily crossed this boundary and then further grew along the main dendrites in the dilution zone of the Alloy 182 weld metal parallel to the solidification direction (and therefore perpendicular to the fusion boundary), which caused a deflection of the SCC crack plane by an angle of 45 to 90° at the fusion boundary. The resulting mixed mode loading in combination with the high surface roughness then resulted in a

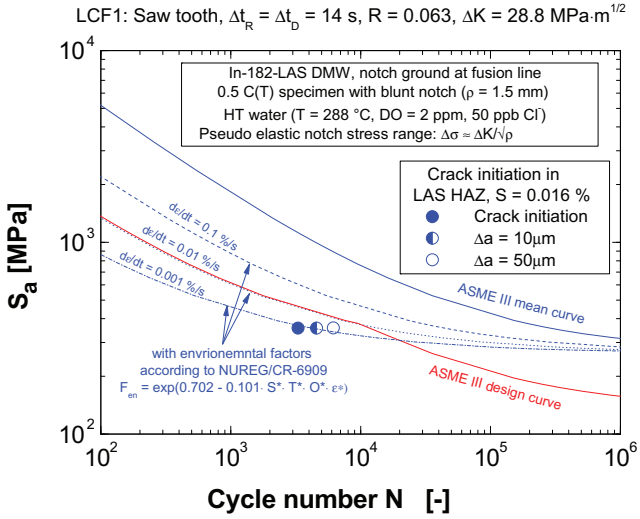

Fig. 22. Comparison of the numbers of fatigue cycles to crack initiation in the region of the HAZ of the low-alloy RPV steel in the blunt notch dissimilar metal weld specimen MN ST 6 in oxygenated high-temperature water with the ASME III mean and design curve for LAS [33,34] [see also Fig. 19(b)].

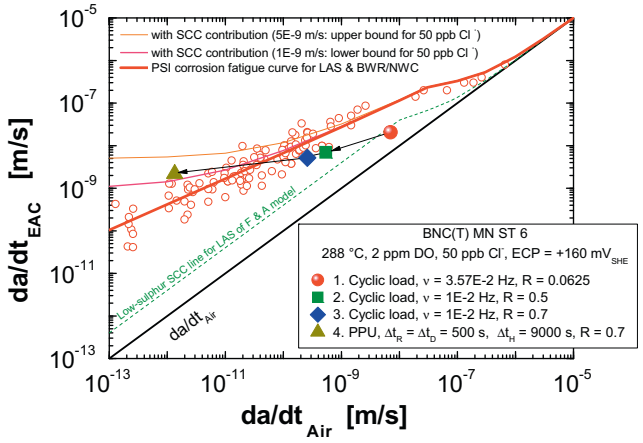

Fig. 23. Comparison of the corrosion fatigue and SCC crack growth rates in the LAS HAZ of the blunt-notched dissimilar metal weld specimen MN ST 6 under cyclic and periodical partial unloading conditions in oxygenated high-temperature water with 50 ppb chloride with corresponding crack growth curves, which were developed for homogeneous LAS specimens [7].

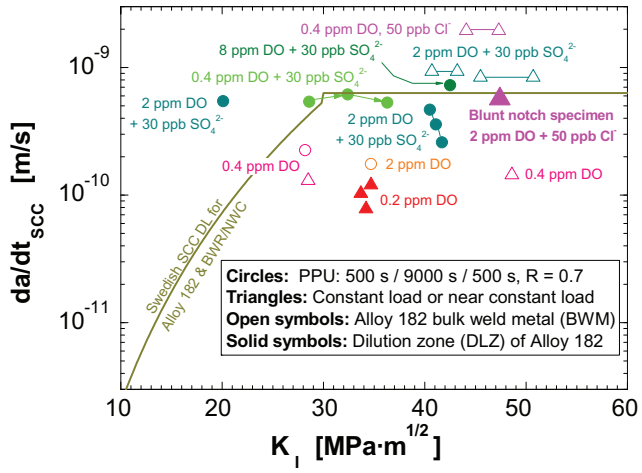

Fig. 25. Comparison of the SCC growth rates in the dilution zone of the Alloy 182 weld metal of the blunt-notched dissimilar metal weld specimen MN ST 6 with results from homogeneous and dissimilar metal weld specimens under similar testing conditions.

crack closure induced cessation of the SCC crack growth in this region at most locations of the crack front (Fig. 24). After a load increase, the crack in the dilution zone of the Alloy 182 weld metal close to the fusion boundary re-started to grow. The SCC crack growth rate was thereby in the typical range for Alloy 182 under these test conditions (Fig. 25).

3.3. SCC behaviour of the Alloy 182 bulk weld metal

The SCC crack growth rates in the Alloy 182 bulk weld metal parallel to the solidification direction in high-purity water were only slightly higher than in the Alloy 182 dilution zone and slightly below the current Swedish SCC disposition line for Alloy 182 and BWR/NWC conditions, which further confirms the adequacy and conservatism of this disposition line (Figs. 7 and 25). A plateau SCC cracking behaviour was observed above a K_I-value of 20–25 MPa · $m^{1/2}$, i.e., the SCC crack growth rates were independent of the applied K_I [Figs. 7, 25 and 26(a)]. The SCC crack growth rates

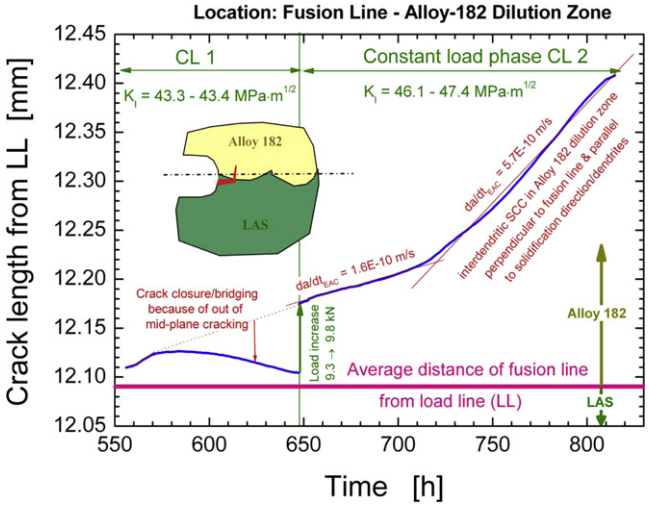

Fig. 24. Apparent cessation of interdendritic SCC growth in the dilution zone of the Alloy 182 weld metal of the blunt-notched dissimilar metal weld specimen MN ST 6 briefly after crossing the fusion boundary because of crack closure and re-establishment of sustained SCC with growth rates in the typical range for Alloy 182 weld metal after a small load increase.

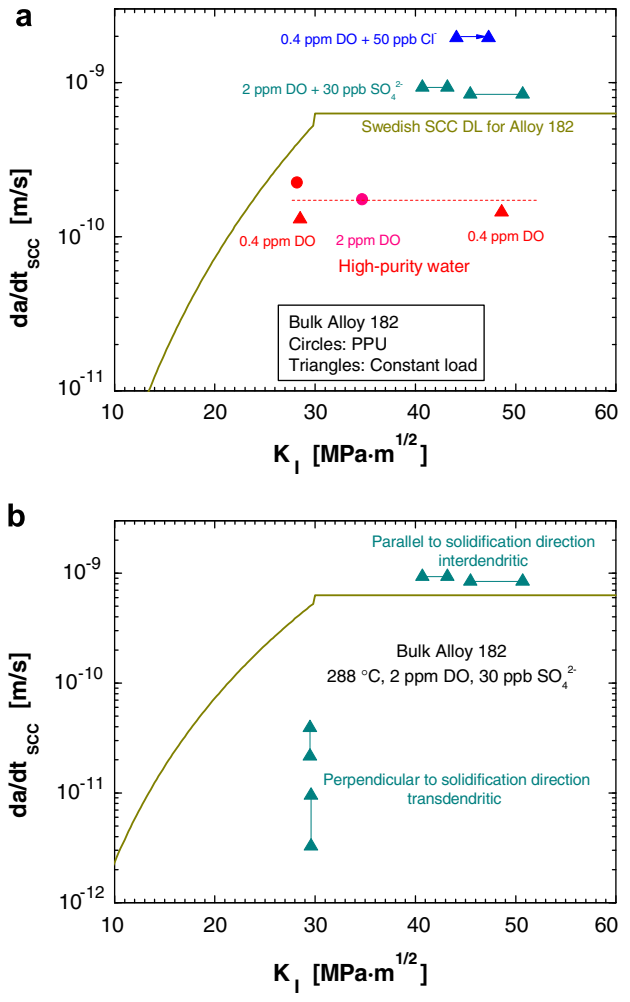

Fig. 26. (a) Interdendritic SCC crack growth rates in the Alloy 182 bulk weld metal in high-purity water and water with 30 ppb of sulphate or 50 ppb of chloride. (b) Trans- and interdendritic SCC crack growth rates in the Alloy 182 bulk weld metal perpendicular and parallel to the solidification and primary dendrite axis, respectively.

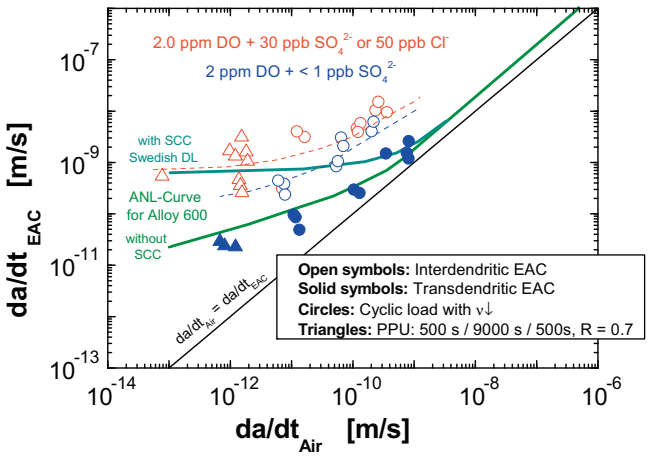

Fig. 27. Comparison of trans- and inter-dendritic corrosion fatigue crack growth rates in Alloy 182 weld metal perpendicular and parallel to the solidification axis in oxygenated high-temperature water with the ANL corrosion fatigue curve for wrought Alloy 600 [39] and a modified curve, which includes an additional SCC contribution at low-loading frequencies or high-load ratios.

in the Alloy 182 bulk weld metal parallel to the solidification direction in oxygenated high-temperature water with 50 ppb Cl^- or 30 ppb SO_4^{2-} were about a factor of 10 and 5 higher than in high-purity water and slightly higher than the Swedish SCC disposition line for Alloy 182 [Fig. 26(a)] [31]. The transdendritic EAC crack growth rates under periodical partial unloading perpendicular to the solidification direction were more than a factor of 10 lower than the corresponding interdendritic EAC crack growth rates parallel to the solidification direction [Fig. 26(b)].

3.4. Corrosion fatigue behaviour of the Alloy 182 bulk weld metal

A higher corrosion fatigue initiation susceptibility was observed in the LAS HAZ than in the dilution zone of the Alloy 182 bulk weld metal (see Section 3.2). In good agreement with wrought Alloy 600 and in contrast to LAS [34], only a very minor environmental reduction of fatigue life was observed in Alloy 182 under BWR/NWC conditions (Fig. 18). On the other hand, significant environmental acceleration of fatigue crack growth of mechanically long cracks was observed in Alloy 182 weld metal under BWR/NWC conditions at loading frequencies below 0.1 Hz (Figs. 20 and 27). The environmental acceleration increased with decreasing loading frequency. The transdendritic corrosion fatigue crack growth rates under cyclic load perpendicular to the solidification axis were a factor of 5–10 lower than the corresponding interdendritic corrosion fatigue crack growth rates parallel to the solidification axis and in a similar range for the wrought Alloy 600 and the ANL-curve for Alloy 600 [39] (Fig. 27). Interdendritic corrosion fatigue crack growth rates in Alloy 182 under cyclic load were significantly higher (a factor of 10) than in wrought Alloy 600 and the ANL-curve for Alloy 600 (Fig. 27).

4. Summary and conclusions

Recent SCC incidents in the weld metal of bottom head penetration housing and core shroud support welds of BWR have drawn the attention to the SCC behaviour in the transition region of Alloy 182-LAS dissimilar weld joints, and in particular, to the issue whether an intergranular/interdendritic SCC crack propagating in the weld metal could easily penetrate through the fusion line into the adjacent low-alloy RPV steel. In order to improve the understanding of the SCC behaviour in the transition region, the SCC crack growth behaviour in the transition region of a simulated Alloy 182-SA 508 Cl.2 weld joint was investigated under simulated BWR/NWC conditions at FRI and PSI.

The main conclusions of these experimental investigations can be summarized as follows [3,7]: The observed EAC cracking behaviour correlates excellently with the field experience, where SCC cracking was usually confined to the Alloy 182 weld metal and no cases of SCC were observed in LAS primary pressure boundary components. The fusion boundary seems to represent a significant barrier for SCC crack growth from the Alloy 182 to the RPV steel, but minor crack growth into the adjacent RPV steel is not impossible. Under static loading conditions in chloride-free, high-temperature water, there seems to be little risk, that a fast growing interdendritic SCC crack may cross the fusion line and significantly propagate into the adjacent low-alloy RPV steel. Even if a crack would cross the fusion line under static load, it is anticipated that cessation of SCC occurs in the LAS HAZ or at the latest in the unaffected LAS base material. Major EAC crack propagation into the RPV material is therefore not expected as long as the number of plant transients is limited and severe and prolonged chloride excursions are avoided (i.e., if water chemistry is kept below the EPRI action level 1 limit).

These important conclusions should be verified by further tests with additional dissimilar weld joints representing different welding qualities and different LAS base materials (steel sulphur content and DSA susceptibility). Since the stress intensity factor in the interface region of dissimilar metal welds can reach quite high levels in some field situations, such investigations should also include experiments in the K_I-range of 50–70 MPa · $m^{0.5}$ with chloride levels below 5–10 ppb, which requires the use of sufficiently large specimens. Because of the safety concern in case of SCC in the RPV, the special emphasis of these evaluations should be placed to a better establishment of the K_I-thresholds, where the onset of fast SCC in LAS may occur.

The observed interface cracking behaviour should also be verified by some few experiments under primary PWR water conditions at higher temperatures of 320 °C, although the situation is rather relaxed here, because of the very low SCC and moderate corrosion fatigue susceptibilities of LAS at low ECP.

Acknowledgments

The results of this paper were generated within a co-operation work between the Fracture & Reliability Research Institute (FRI) and Paul Scherrer Institute (PSI) and are a part of the PEACE-II/III (FRI) and RIKORR-II/KORA (PSI) programs. The financial support of the PEACE-II/III program by EdF, EPRI, Hitachi, JAPCO, KEPCO, MHI, SKI, Tohoku EPCO, TEPCO, TEPCO, Toshiba and IHI and of the RIKORR-II/KORA program by the Swiss Federal Nuclear Safety Inspectorate (HSK) and Swiss Federal Office for Energy (BFE) is gratefully acknowledged. Thanks are also expressed to B. Baumgartner, L. Nue, U. Ineichen, U. Tschanz, B. Gerodetti and E. Groth (all PSI) for their experimental contribution to this work.

Appendix A

A.1. Metallurgical and microstructural aspects of SCC in Alloy 182 weld metal

Manually welded multipass dissimilar weld joints usually have a complex welding configuration (e.g., safe ends with cladding and weld butter) and microstructure, which may significantly differ from weld to weld depending on welding parameters. During solidification, parallel bundles of dendrites with nearly identical crystallographic orientation form and grow into the melt along the direction of heat flux. The boundaries between these similarly

oriented dendrites are often called solidification subgrain boundaries (SSGB) and tend to have low-angular mismatches, as well as low energy. Where different bundles of dendrites intersect or overlap, larger angular mismatches often occur between the grains of the bundles. In this case, the resulting high-angle grain boundaries, termed solidification grain boundaries (SGB), can be high-energy random grain boundaries or low-energy coincident site lattice (CSL) boundaries. SGB can migrate on cooling after solidification and during re-heating and result in a straighter, migrated grain boundary (MGB) [20].

The general structure of an individual weld pass consists of elongated columnar dendrites at the edge of the melt pool, where heat transfer is highly directional, and more equiaxed cellular dendrites in the middle with slower cooling. During solidification, the dendrite arms grow towards each other and trap enriched (with S, P, Si, Mn and Nb) liquid in the interstices along with melt oxides and slag inclusions. Therefore, Mn and Nb segregation is often observed in the grains and the grain boundaries are usually decorated with precipitates (carbides) and enriched with S, P and Si. Each weld pass heats up the layers below and can cause recrystallization and migration of SGB, segregation, precipitation (e.g., carbides) or hot cracking and produce a wide range of microstructures potentially susceptible to SCC [8,20].

PWHT of the weld buttering is a standard practice, and PWHT is in some cases also performed on the weld filler metal following final welding. In addition, PWHT often occurs indirectly as a consequence of stress relief heat treatment performed on adjacent LAS components, but in this case the stress relief temperature is well below the optimum for the more creep/relaxation resistant nickel base alloys. While stress relief treatment only slightly reduces the peaks in residual stress, it can produce some elevation in yield strength/hardness and potentially exacerbate Cr depletion/sensitization by carbide precipitations, which both may further increase the SCC susceptibility of this region [8]. As-welded structures are thus usually less sensitized than welds, which were PWHT, although both behaved very similarly in lab SCC CGR studies [8]. In-service thermal ageing might further exacerbate SCC susceptibility [2].

The grain boundary chemistry and misorientation in the weld metal as well as the S, P, Si and Cr content and the stabilization ratio (Nb + Ti vs. C content) were material factors, which affected the SCC cracking behaviour in the Alloy 182 weld metal [2,8–10]:

S and Si grain boundary segregation affects the anodic dissolution and repassivation behaviour at the grain boundaries and/or can result in decohesion and grain boundary weakening. The high-angle random boundaries are prone to segregation and precipitation, while low-energy boundaries, such as low-angle boundaries, are not [10]. Furthermore, the strong mismatch in Taylor factor in high-angle boundaries favours a higher strain incompatibility and grain boundary deformation and therefore further promotes IG/ID cracking [11]. Low-angle boundaries are more resistant to SCC than high-angle coincident and random boundaries, the latter being the least resistant [10]. The different susceptibilities are also the main reason for crack pinning phenomena and uneven crack fronts in SCC lab testing.

SCC cracks in weld metals typically follow the higher energy random SGB and/or MGB [20]. The orientation of the crack in the weld, i.e., relative to the weld's columnar microstructure, has a strong influence on the crack growth rate. Cracks grow fastest along high-energy grain boundaries in the direction of main dendrite growth, and next fastest along high-energy grain boundaries perpendicular to the direction of dendrite growth but parallel to the welding direction [20]. Cracks that grow perpendicular to the high-energy grain boundaries, i.e., perpendicular to the columnar dendrites, grow significantly more slowly. In the interface region between the weld metal and the heavy-section LAS structures, the main dendrite growth direction is perpendicular to the fusion line according to the heat-flux during welding [20].

Cr strongly affects the SCC behaviour in Ni-base alloys since it significantly improves their corrosion resistance and repassivation behaviour. Cr has a high affinity to C and readily forms carbides such as $Cr_{23}C_6$ or Cr_7C_3, which can precipitate at grain boundaries. This may result in Cr depletion in a narrow zone close to the grain boundary (sensitization) and concurrent higher susceptibility to IG corrosion and IG SCC at high ECP (BWR/NWC), although this effect is less pronounced than in stainless steels [2,8]. The problem of Cr depletion can be reduced by either increasing the chromium content or by introducing elements with high affinity to C like Nb and Ti, which form very stable carbides. This aspect is reflected by the SCC resistance index SCRI [43] in Eq. (1), which is used by the BWR vendors to characterize the SCC susceptibility of Ni-alloys.

$$\mathrm{SCRI} = \mathrm{Cr} + (\mathrm{Nb} + \mathrm{Ta}) \cdot 5 + \mathrm{Ti} \cdot 10 - 116.5 \cdot \mathrm{C} \quad (1)$$

In wrought Alloy 600, grain boundary carbide improved its IG SCC resistance, which has been related to the reduction in grain boundary sliding. Such correlations were not observed in Alloy 182 weld metals [44].

Carbon strongly affects the mechanical properties and yield strength of the material by primary (MC, etc.) and secondary carbide ($M_{23}C_6$, etc.) precipitation. A higher C content usually results in a higher high-temperature yield strength, which may make the alloy more susceptible to SCC (steeper strain gradient and higher crack-tip strain rate) and low-temperature rapid crack propagation, and produce high weld residual stresses and stress intensity factors. On the other hand, high carbon content also favours sensitization. Similarly to yield strength, cold work (e.g., from surface grinding or weld shrinkage strain, etc.) also increases SCC crack growth rates and susceptibility at high (BWR/NWC) and low ECP (PWR, BWR/HWC) [8].

A.2. Metallurgical and microstructural aspects of SCC in the interface region between the Alloy 182 weld and LAS base metal

In the transition region between the Alloy 182 weld metal and the LAS a very complex microstructure with varying chemical composition can evolve, e.g., due to dilution of alloying elements between the Alloy 182 weld filler and LAS base metal during welding or the migration of C from the LAS to the weld metal during PWHT: In the weld metal close to the fusion line, a few mm thick zone with different chemical composition from the mixing of the weld filler material with the molten LAS is observed. The reduced Cr (and Ni) content in this dilution zone close to the LAS tends to increase its corrosion and SCC susceptibility (e.g., by the effect of Cr on the repassivation behaviour) with respect to the bulk weld metal. The local formation of a very narrow and hard layer of martensite on cooling in the weld metal adjacent to the fusion boundary is possible, but requires a very high dilution and is thus much less frequently observed than in stainless steel weld filler materials.

As a consequence of the C migration, PWHT can potentially produce a more distinct elevation in yield strength/hardness and more severe Cr depletion/sensitization both by carbide precipitations in the interface region compared to the bulk weld metal, which both may further increase the SCC susceptibility of this region. A further consequence of C diffusion is that the LAS may become slightly decarburized in a zone adjacent to the fusion boundary in severe cases. This decarburized zone may be softer and may have a lower yield strength than the parent LAS, and therefore a potentially higher susceptibility to SICC during plant transients, but increased SCC resistance under stationary operating conditions. The LAS weld HAZ of dissimilar weld joints usually has a lower peak

hardness ($\leqslant$ 300 HV5) than in welds between LAS components ($\leqslant$ 350 HV5).

The moderately different thermal expansion coefficient of Alloy 182 and LAS may produce thermal fit-up stress at the interface during start-up/shut-down and also at operating temperature and thus result in a change of the acting stress intensity factor in the field, although the situation is much less severe than with stainless steel weld filler metals.

Significant galvanic effects are not expected, since the ECP of the LAS in BWR/NWC environment is only slightly lower (50–100 mV) than that of Alloy 182 and since the throwing power is very limited in high-purity (very low conductivity) water.

References

[1] R.M. Horn, P.L. Andresen, J. Hickling, BWR Alloy 182 stress corrosion cracking experience, in: Proceedings of the Fifth International Symposium on Contribution of Materials Investigation to the Resolution of Problems Encountered in Pressurized Water Reactors (Fontevraud 5), Cd-ROM, Fontevraud, France, 23–27 September 2002, p. 55.

[2] H. Hänninen et al., Dissimilar metal weld joints and their performance in nuclear power plant and oil refinery conditions, VTT Research Notes 2347, VTT, Espoo, Finland, 2006. <http://www.vtt.fi/inf/pdf/tiedotteet/2006/T2347.pdf>.

[3] R.S. Pathania, A.R. McIlree, J. Hickling, Overview of primary water cracking of Alloys 182/82 in PWRs, in: Proceedings of the Fifth International Symposium on Contribution of Materials Investigation to the Resolution of Problems Encountered in Pressurized Water Reactors (Fontevraud 5), CD-ROM, Fontevraud, France, 23–27 September 2002, p. 13.

[4] T. Matsunaga, K. Matsunaga, Stress corrosion cracking of CRD stub tube joint and repair at Hamaoka Unit 1, in: Proceedings of Eleventh International Conference on Nuclear Engineering, Paper ICONE11-36056, Shinjuku, Tokyo, Japan, 20–23 April 2003.

[5] A. Yamashita, K. Takeuchi, W. Sagawa, F. Manabe, The stress corrosion cracking at shroud support Tsuruga Unit 1, in: Proceedings of Ninth International Conference on Nuclear Engineering, Paper ICONE 9–66, 8–12 April 2001, Nice, France.

[6] H.P. Seifert, S. Ritter, J. Nucl. Mater. 372 (2008) 114.

[7] H.P. Seifert, S. Ritter, Research and service experience with environmentally-assisted cracking of carbon and low-alloy steels in high-temperature water, SKI-Report 2005:60, Stockholm, Sweden, 2006. <www.ski.se>.

[8] P.L. Andresen, L.M. Young, P.W. Emigh, R.M. Horn, Stress corrosion crack growth rate behavior of Ni Alloys 182 and 600 in high temperature water, NACE Corrosion 2002, CD-ROM, Paper No. 02510, NACE, 2002.

[9] Q.J. Peng, H. Yamauchi, T. Shoji, Metall. Mater. Trans. A 34A (9) (2003) 1891.

[10] Q. Peng et al., Corros. Sci. 49 (2007) 2767.

[11] B. Alexandreanu, O.K. Chopra, W.J. Shack, The effect of grain orientation on the cracking behaviour of Alloy 182 in PWR environment, in: Proceedings of the Twelfth International Conference on Environmental degradation of Materials in Nuclear Power Systems – Water Reactors, Snowbird, Utah, USA, TMS, 14–18 August 2005, p. 579.

[12] P. Scott et al., Examination of stress corrosion cracks in Alloy 182 weld metal after exposure to PWR primary water, in: Proceedings of the Twelfth International Conference on Environmental degradation of Materials in Nuclear Power Systems – Water Reactors, TMS, Snowbird, UT, August 14–18 2005, p. 497.

[13] P. Andresen, Corrosion 44 (1988) 376.

[14] M. Itow et al., Crack growth rates of Alloy 182 in high temperature water, in: Proceedings of the Seventh International Conference on Environmental degradation of Materials in Nuclear Power Systems – Water Reactors, NACE International, Houston, TX, 1995, p. 541.

[15] M. Itow et al., The effect of corrosion potential on Alloy 182 crack growth rate in high temperature water, in: Proceedings of the Eighth International Conference on Environmental degradation of Materials in Nuclear Power Systems – Water Reactors, ANS, La Grange Park, IL, 1997, p. 712.

[16] R. Lindström, P. Lidar, J. Lagerström, Crack growth of Alloy 182 in a simulated primary side PWR environment, in: Proceedings of the Eighth International Conference on Environmental degradation of Materials in Nuclear Power Systems – Water Reactors, ANS, La Grange Park, IL, 1997, p. 422.

[17] W.H. Bamford, J.P. Foster, R.S. Pathania, An investigation of Alloy 182 stress corrosion cracking in simulated PWR environment, in: Proceedings of the Ninth International Conference on Environmental degradation of Materials in Nuclear Power Systems – Water Reactors, TMS, Warrendale, PA, 1999, p. 279.

[18] T. Cassagne et al., Stress corrosion crack growth rate measurements in Alloys 600 and 182 in primary water loops under constant load, in: Proceedings of the Ninth International Conference on Environmental degradation of Materials in Nuclear Power Systems Water Reactors, TMS, Warrendale, PA, 1999, p. 217.

[19] S.L. Hong et al., Measurements of stress corrosion cracking growth rates in weld Alloy 182 in primary water of PWR, in: Proceedings of the Tenth International Conference on Environmental degradation of Materials in Nuclear Power Systems – Water Reactors, NACE, Houston, TX, 2001, CD-ROM.

[20] G.A. White et al., Development of crack growth rate disposition curves for primary water stress corrosion cracking (PWSCC) of Alloy 82, 182 and 132 weldments, in: Proceedings of the Twelfth International Conference on Environmental degradation of Materials in Nuclear Power Systems – Water Reactors, TMS, Snowbird, UT, 2005, p. 511.

[21] D.R. Tice et al., Evaluation of test techniques for stress corrosion cracking of dissimilar weldments, in: Proceedings of the Tenth International Conference on Environmental degradation of Materials in Nuclear Power Systems Water Reactors, 2001, Cd-ROM, ANS/TMS/NACE, Lake Tahoe, Nevada, USA, 5–9 August, 2001.

[22] G.F. Li, J. Congleton, Corros. Sci. 42 (2000) 1005.

[23] P. Hurst, A.S. Raffel, D.R. Tice, Environmental degradation of dissimilar metal welds, in: Proceedings of the Eighth International Conference on Environmental degradation of Materials in Nuclear Power Systems – Water Reactors, vol. 1, ANS, Amelia Island, FL, USA, 10–14 August 1999, p. 430.

[24] M. Ruscak et al., Int. J. Pres. Vessel Pip. 68 (1996) 23.

[25] R. Page, Corrosion 41 (1985) 338.

[26] ASTM E399-06, Standard test method for linear-elastic plane-strain fracture toughness K_{IC} of metallic materials, Annual Book of ASTM Standards, Section 3, vol. 03.01, ISBN 978-0-8031-4310-4, ASTM International, 2007, p. 520.

[27] K. Reichlin, 2-D FE calibration of DCPD for a bimetallic weld joint, Paul Scherrer Institute, unpublished work.

[28] P.M. Yukawich, C.W. Hughes, C.W. Practical, Metallography 15 (1978) 399.

[29] ASTM E647-05, Standard test method for determining threshold stress intensity factor for environment-assisted cracking of metallic materials, Annual Book of ASTM Standards, Section 3, vol. 03.01, ISBN 978-0-8031-4310-4, ASTM International, 2007, p. 1067.

[30] ASTM E1681-03, Standard test method for measurement of fatigue crack growth rates, Annual Book of ASTM Standards, Section 3, vol. 03.01, ISBN 978-0-8031-4310-4, ASTM International, 2007, p. 692.

[31] Personal communication with C. Jansson (SwedPower AB).

[32] F.P. Ford et al., Stress corrosion cracking of low alloy steels under BWR conditions, assessments of crack growth rate algorithms, in: Proceedings of the Ninth International Conference on Environmental degradation of Materials in Nuclear Power Systems – Water Reactors, ANS/NACE/TMS, Newport Beach, CA, 1–5 August 1999, p. 855.

[33] The 2004 ASME Boiler and Pressure Vessel Code, Section III, Subsection NB, Appendix I, The American Society of Mechanical Engineers, New York, USA, 2004.

[34] O.K. Chopra, W.J. Shack, Effect of LWR coolant environment on the fatigue life of reactor materials, Final report, NUREG/CR-6909, ANL-06/08, US NRC, Washington, DC, USA, February 2007. <http://adamswebsearch.nrc.gov/scripts/securelogin.pl>.

[35] C.E. Jaske, W.J. O'donnell, J. Pres. Vessel Technol. 99 (1977) 584.

[36] W.K. Wilson, J. Pres. Vessel Technol. 96 (1974) 293.

[37] H.P. Seifert, S. Ritter, Corros. Sci, 2008, doi:10.1016/j.corsci.2008.03.010.

[38] E. Eason et al., Nucl. Eng. Des. 184 (1998) 89.

[39] O.K. Chopra, W.K. Soppet, W.J. Shack, Effects of cold work, and water chemistry on corrosion fatigue and stress corrosion cracking of nickel alloys and welds, NUREG/CR-6721, ANL/01/07, US NRC, Washington, DC, USA, April 2001.

[40] P.L. Andresen, Corrosion 47 (12) (1991) 917.

[41] F.P. Ford, P.L. Andresen, Corrosion fatigue of A533B/A508 pressure vessel steels in 288 °C water, in: Third International IAEA Specialist's Meeting on Subcritical Crack Growth, vol. 1, W. Cullen (Ed.), NUREG/CP-0112, Moscow, USSR, 14–17 May 1990, p. 105.

[42] F.P. Ford, P.L. Andresen, Stress corrosion cracking of low-alloy steels in 288 °C water, NACE Corrosion 1989, NACE, New Orleans, Houston, USA, Paper No. 498, p. 498-1.

[43] K. Yamauchi et al., Nucl. Eng. Des. 129 (1991) 321.

[44] C. Amzallag et al., Stress corrosion life experience of 182 and 82 welds in French PWRs, in: Proceedings of the Fifth International Symposium on Contribution of Materials Investigation to the Resolution of Problems Encountered in Pressurized Water Reactors (Fontevraud 5), Cd-ROM, Fontevraud, France, 23–27 September 2002, p. 69.